HHS Public Access

Author manuscript

Small. Author manuscript; available in PMC 2017 December 01.

Published in final edited form as:

Small. 2016 December ; 12(46): 6353–6362. doi:10.1002/smll.201601597.

Facile Fabrication of Tumor Redox-Sensitive Nanoassemblies of Small-Molecule Oleate Prodrug as Potent Chemotherapeutic Nanomedicine

Cong Luo,
Department of Pharmaceutics, School of Pharmacy, Shenyang Pharmaceutical University, Shenyang 110016, PR China

Jin Sun,
Municipal Key Laboratory of Biopharmaceutics, School of Pharmacy, Shenyang Pharmaceutical University, Shenyang 110016, PR China

Bingjun Sun,
Department of Pharmaceutics, School of Pharmacy, Shenyang Pharmaceutical University, Shenyang 110016, PR China

Dan Liu,
Key Laboratory of Structure-Based Drug Design and Discovery, Shenyang Pharmaceutical University, Shenyang 110016, PR China

Lei Miao,
Division of Molecular Pharmaceutics and Center of Nanotechnology in Drug Delivery, Eshelman School of Pharmacy, University of North Carolina at Chapel Hill, Chapel Hill, NC 27599, USA

Tyler Jay Goodwin,
Division of Molecular Pharmaceutics and Center of Nanotechnology in Drug Delivery, Eshelman School of Pharmacy, University of North Carolina at Chapel Hill, Chapel Hill, NC 27599, USA

Leaf Huang, and
Division of Molecular Pharmaceutics and Center of Nanotechnology in Drug Delivery, Eshelman School of Pharmacy, University of North Carolina at Chapel Hill, Chapel Hill, NC 27599, USA

Zhonggui He
Department of Pharmaceutics, School of Pharmacy, Shenyang Pharmaceutical University, Shenyang 110016, PR China

Abstract

The conjugate of paclitaxel (PTX) and docosahexaenoic acid has entered into clinical trials. However, the most recent clinical outcomes fell short of expectations, due to the extremely slow drug release from the hydrophobic conjugates. Herein, we report a novel prodrug-based nanoplatform self-assembled by the disulfide bond linked conjugates of PTX and oleic acid (OA)

Correspondence to: Jin Sun; Zhonggui He.

Supporting Information

Supporting Information is available from the Wiley Online Library or from the author.

for rapid and differential release of PTX in tumor cells. This redox-responsive prodrug-nanosystem demonstrates multiple therapeutic advantages, including one-step facile fabrication, high drug-loading efficiency (56%, w/w), on-demand drug release responding to redox stimuli, as well as favorable cellular uptake and biodistribution. These advantages result in significantly enhanced antitumor efficacy *in vivo*, with the tumor almost completely disappearing in mice. Such a uniquely engineered prodrug-nanosystem has great potential to be used as potent chemotherapeutic nanomedicine in clinical cancer therapy.

Graphical Abstract

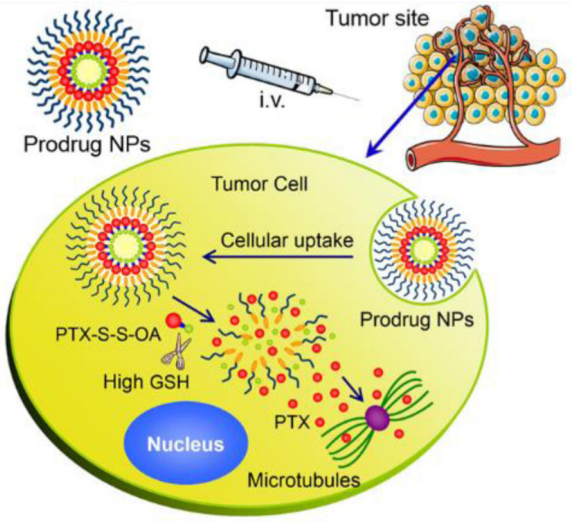

To bridge the gap between hydrophobic lipid prodrugs of PTX and favorable antitumor efficacy, a smart redox-sensitive prodrug-nanosystem has been designed. The uniquely engineered stimulus-responsive prodrug nanoassemblies, with high drug loading (over 50%, w/w), on-demand drug release within tumor cells and potent antitumor efficacy, hold great potential to be used as a promising chemotherapeutic nanomedicine in cancer therapy.

Keywords

paclitaxel; disulfide bond; oleate prodrug; prodrug-nanosystem; cancer therapy

1. Introduction

Although the fields of nanotechnology and biomaterials have been extensively explored for anticancer drug delivery, the clinical outcomes of the available nanoparticulate drug delivery systems (Nano-DDS) were not as good as expected.[1–3] The limiting clinical efficacy of these conventional Nano-DDS can be attributed to several disadvantages, including low drug-loading capacity (<10%, w/w), poor stability, potential crystallization during storage, premature drug leakage from vehicles, and serious excipient-induced toxicity.[4] Therefore, it's necessary to develop high-efficiency vehicles for systemic delivery of anticancer drugs.

Fatty acids, especially unsaturated fatty acids (UFAs), have been widely used to develop fatty acids-based conjugates for healthcare applications.[5–7] For cancer therapy, a wide range of conjugates based on UFAs have been designed for anticancer drug delivery. Among them, three conjugates have entered clinical trials and hold a great potential to be applied in clinicals in the future, including docosahexaenoic acid (DHA)-PTX, Elaidic acid-cytarabine and Elaidic acid-gemcitabine.[8–10] The rational design of UFAs-based conjugates can be attributed to the following aspects: (i) to enhance the stability of anticancer drugs,[10, 11] the conjugation of anticancer drugs with UFAs can protect the fragile groups of the parent drug from being metabolized *in vivo*; (ii) to improve lipophilicity of drugs,[11] hydrophilic drugs can not easily pass through the bilayer membrane via passive diffusion, resulting in poor bioavailability in target sites; (iii) to achieve natural targeting effects to tumors,[12,13] several studies have suggested an increased fatty acid uptake in tumors as nutrient sources; (iv) to enhance the chemotherapeutic response of anticancer drugs,[14–17] some UFAs could significantly sensitize anticancer drugs-induced apoptosis of human tumor cells; and (v) to minimize side effects of anticancer drugs at high doses,[18] low cytotoxicity and sustained release of the parent drugs make UFAs-based anticancer conjugates reduced side effects. Therefore, developing advanced UFAs-based DDS holds great potential for cancer therapy.

Paclitaxel (PTX) has been widely utilized in clinic for the treatment of a wide range of cancer, including non-small cell lung cancer, breast cancer, ovarian cancer, and malignant melanoma.[19] The antitumor mechanism of PTX can be attributed to interacting with microtubules to prevent depolymerization.[20] Taxol, the first commercially available formulation of PTX, has long been criticized for its serious excipient-associated toxicities. In response to these problems, various drug delivery strategies have been developed to improve the drug availability and to enhance the antitumor efficiency of PTX, including designing prodrugs and Nano-DDS.[4,21] Among these strategies for PTX delivery, lipid prodrugs of PTX and fatty acids have been widely investigated. The conjugate of PTX and DHA has been under phase III clinical trials.[8,22] Unfortunately, PTX-DHA showed no significant advance in inhibiting tumor growth of patients in clinical trials,[8] due to the inefficient release of PTX from the hydrophobic conjugate.[18]

Tumor cells are characterized as elevated intracellular glutathione (GSH) level, and the cytosolic GSH concentration in tumor cells is several times higher than that in normal cells.[23,24] The elevated GSH level in tumor cells has been extensively explored for designing stimulus-sensitive Nano-DDS, and disulfide bond has been widely used as a redox-responsive linkage to facilitate a rapid and differential release of anticancer drugs in tumor cells.[24,25] We thereby hypothesized that designing a disulfide bond inserted prodrug of PTX and fatty acids would facilitate the rapid and differential release of free PTX from hydrophobic conjugates.

Based on this rationale, a novel redox-responsive conjugate of PTX and oleic acid (OA), denoted as PTX-S-S-OA, was synthesized by covalently connecting PTX and OA via a disulfide bond. An ester prodrug (PTX-OA) was synthesized as the non-sensitive conjugate. The unsaturated alkyl chains of UFAs, e.g. OA in these two conjugates, would benefit the sufficient structural flexibility conferred by the double bond of OA. However, some UFAs with too many double bonds (e.g. DHA with six double bonds) would be more easily

oxidized and degraded, resulting in inferior chemical stability of UFAs-based conjugates. In addition, it has been reported that the combination of OA and PTX can significantly enhance the chemosensitivity of PTX.[15] That's the reason why OA was selected for the rational design of PTX conjugates in the present study. Interestingly, both PTX-S-S-OA and PTX-OA could self-assemble into nanoparticles (NPs) in deionized water. Therefore, a novel prodrug-nanosystems was developed by integrating prodrug strategy and nanotechnology into one system to facilitate systemic delivery of PTX. Tocopheryl polyethylene glycol 2000 succinate ($TPGS_{2k}$) was added to the prodrug-nanosystem for improved colloidal stability and prolonged blood circulation. The PEGylated prodrug nanoassemblies of PTX-S-S-OA (PTX-S-S-OA/$TPGS_{2k}$ NPs), demonstrated significantly high drug loading (56% of PTX, w/w) as well as on-demand drug release responding to redox stimuli. After internalization into the tumor cells, the elevated intracellular glutathione (GSH) level triggers the cleavage of the disulfide bond,[23] resulting in the rapid and differential release of PTX. Which in turn facilitate PTX-induced apoptosis of tumor cells. The high drug loading efficiency and rapid release of free PTX from the hydrophobic conjugate within the tumor cells would significantly improve the therapeutic efficacy. Although disulfide bond has been widely used as redox-sensitive linkage for designing anticancer conjugates,[25–27] including PTX conjugates, to our knowledge, this is the first attempt to develop prodrug-nanoplatform based on disulfide bond-bridged hydrophobic conjugates of PTX and fatty acids for systemic delivery of PTX. In such a uniquely engineered prodrug-nanosystem, prodrug strategy and nanotechnology are integrated into one system to facilitate the chemotherapy efficiency of PTX.

2. Results and Discussions

2.1 Design and Synthesis of Prodrugs

To test our hypothesis, a novel redox-sensitive PTX-fatty acid conjugates (PTX-S-S-OA) was synthesized by conjugating OA to PTX via disulfide bond as a linkage (Scheme S1). Additionally, OA was directly coupled to the C2'-oxygen of paclitaxel via a simple ester bond to obtain an ester prodrug (PTX-OA). The chemical structures of PTX-S-S-OA and PTX-OA were confirmed by MS, ^{1}H NMR and IR (Figure S1and S2).

2.2. Self-Assembly of Prodrugs in Water

A simple nano-precipitation method was used to prepared nanoassemblies. Interestingly, both PTX-S-S-OA and PTX-OA were found to spontaneously assemble into uniform nanoparticles in deionized water. In contrast, when nanoprecipitation was performed utilizing free PTX instead of the fatty acid conjugates, PTX immediately precipitated, suggesting the crucial role of the fatty acid moiety in the self-assembly process. As shown in Figure 1 and Table S1, these prodrug nanoassemblies showed spherical morphology with a diameter of around 100 nm (Figure 1 and S3). The PEGylated formulations (15% of $TPGS_{2k}$, w/w) exhibited a slightly increased particle size of about 10 nm when compared with the non-PEGylated ones (Table S1). Nanoparticles with a size of around 100 nm are supposed to be suitable for enhanced tumor accumulation via the enhanced permeation and retention (EPR) effect.[28] In this precisely engineered prodrug-nanosystem, the conjugates simultaneously play two roles as building blocks for nanostructure and the encapsulated

drug. In other words, the conjugates (PTX-OA and PTX-S-S-OA) themselves act as both carriers and cargos. Additionally, OA only accounts for a small proportion in the whole conjugates due to its low molecular weight (~282) when compared with PTX (~853). As a result, these prodrug nanoassemblies showed impressively high drug loading efficiency (56–66% of PTX, w/w) (Table S1). High drug loading is of a great importance for high therapeutic efficacy and low excipient-associated toxicities. Furthermore, the PEGylated prodrug nanoassemblies (PTX-S-S-OA/$TPGS_{2k}$ NPs and PTX-OA/$TPGS_{2k}$ NPs) were highly stable in PBS (pH 7.4) supplemented with 10% FBS at 37 °C, with no significant variation of their mean diameter over a period of 12 h (Figure S4A). They also showed good physical stability for an extended period of time (3 months) at 4 °C (Figure S4B).

2.3 *In Vitro* Hydrolysis of Prodrugs from Nanoassemblies

Dithiothreitol (DTT), a prevailing GSH simulatant, was utilized to investigate the reductive responsiveness of PTX-S-S-OA/$TPGS_{2k}$ NPs. As shown in Figure 2, less than 27% of PTX was released from PTX-S-S-OA/$TPGS_{2k}$ NPs within 12 h in PBS (pH 7.4) without DTT, but more than 90% of PTX was released within 2 h in the presence of 10 mM DTT. The HPLC profile indicated that the released compound was free PTX (data not shown). By contrast, there was no PTX released from PTX-OA/$TPGS_{2k}$ NPs after 24 h incubation in PBS (pH 7.4) either with or without DTT. These results suggest that the drug release from ester prodrug (PTX-OA) is extremely slow, and designing stimuli-sensitive prodrug is an effective strategy to respond to the extremely slow drug release from the hydrophobic prodrugs of PTX and fatty acids. The rapid and differential drug release within tumor cells would result in enhanced antitumor activity.

2.4 *In Vitro* Cytotoxicity Induced by Released PTX

The *in vitro* cytotoxicity was evaluated in KB-3-1, H460 and OVCAR-8 cells at varying equivalent PTX concentrations using the 3-(4,5-dimethylthiazol-2-yl)-2,5-diphenyl tetrazolium bromide (MTT) assay. As shown in Figure 3A and Figure S5, PTX-OA/$TPGS_{2k}$ NPs exhibited no cytotoxicity in all three cell lines within the studied range of drug concentrations, due to the extremely slow hydrolysis rate of active PTX molecules (Figure 2C). By contrast, PTX-S-S-OA/$TPGS_{2k}$ NPs showed comparable cytotoxicity with Taxol, despite of the slightly delayed release of the PTX in tumor cells. These results confirm our hypothesis that the poor clinical outcomes of ester prodrugs of PTX and fatty acid could be attributed to the extremely slow drug release from ester prodrugs (PTX-DHA and PTX-OA). The cytotoxicity of prodrug nanoassemblies highly depends on the release rate of active PTX molecules from prodrugs.

2.5 Cellular Uptake of Prodrug Nanoassemblies

To investigate the cellular uptake, KB-3-1 were incubated with free coumarin-6 (C-6) or C-6-labeled prodrug NPs for different periods of time. After 0.5 h or 2 h of incubation, the cells were observed using confocal microscopy, and the intracellular fluorescence intensity was quantified by Flow Cytometry. As shown in Figure 3B–3D, both C-6-PTX-OA/$TPGS_{2k}$ NPs and C-6-PTX-S-S-OA/$TPGS_{2k}$ NPs exhibited much stronger intracellular fluorescence intensity at 0.5 h and 2 h compared to free C-6, and the intracellular fluorescence intensity significantly increased with time. This indicates that prodrug nanoassemblies elicit a

significantly higher cellular uptake than the free drug. Interestingly, C-6-PTX-S-S-OA/$TPGS_{2k}$ NPs showed much higher intracellular fluorescence intensity than that of C-6-PTX-OA/$TPGS_{2k}$ NPs, despite their similar nanostructure. Indeed, small-molecule prodrug-nanosystem is quite unique, in which prodrugs themselves perform as the carrier materials. Moreover, encapsulation of fluorescent agents into NPs could lead to fluorescence quenching caused by the aggregation-caused quenching (ACQ) effect.[29] After internalization into tumor cells, most C-6 was trapped in C-6-PTX-OA/$TPGS_{2k}$ NPs owing to the high stability of PTX-OA. In contrast, due to the hydrolysis of PTX-S-S-OA in tumor cells, C-6-PTX-S-S-OA/$TPGS_{2k}$ NPs disassembled and released free C-6. As a result, C-6-PTX-S-S-OA/$TPGS_{2k}$ NPs showed higher fluorescence intensity than that of C-6-PTX-OA/$TPGS_{2k}$ NPs.

2.6 Pharmacokinetics

Pharmacokinetics were studied in Sprague Dawley (SD) rats. Taxol, the non-PEGylated prodrug nanoassemblies (PTX-OA NPs and PTX-S-S-OA NPs), and the PEGylated prodrug nanoassemblies (PTX-OA/$TPGS_{2k}$ NPs and PTX-S-S-OA/$TPGS_{2k}$ NPs) were intravenously administrated at an equivalent PTX dose of 5 mg kg^{-1}. As shown in Figure 4, S6 and S7, the non-PEGylated formulations were quickly cleared from blood. The highly hydrophobic surface of non-PEGylated prodrug NPs would lead to rapid identification and phagocytosis by the reticulo-endothelial system (RES). On the other hand, the PEGylated formulations demonstrated significantly prolonged blood-circulation compared to Taxol and the non-PEGylated formulations (Figure 4 and Table S3), owing to the PEG shielding on the outer surface of prodrug NPs. Furthermore, the ester prodrug (PTX-OA) significantly delayed the metabolic process of PTX due to its high chemical stability.[18]. As a result, PTX-OA/$TPGS_{2k}$ NPs exhibited significantly prolonged blood circulation when compared to PTX-S-S-OA/$TPGS_{2k}$ NPs, and most of them were in the form of prodrug (PTX-OA) in blood.

2.7 *In vivo* Biodistribution

We then investigated the biodistribution of prodrug nanoassemblies in KB-3-1 tumor bearing nude mice. Noninvasive optical imaging system (IVIS) was applied for visualization and calculation. When the tumor volume reached 500 mm^3, the mice were administrated intravenously with free DiR and DiR-labeled prodrug nanoassemblies. As shown in Figure 5, free DiR group showed high fluorescent intensity in lung, but very small amount of dye was accumulated in tumor at 24 h. By contrast, both DiR-labeled PTX-S-S-OA/$TPGS_{2k}$ NPs and DiR-labeled PTX-OA/$TPGS_{2k}$ NPs demonstrated strong fluorescent signal in tumor at 24 h, suggesting that prodrug nanoassemblies could successfully accumulate in tumor via passive targeting (EPR effect).

2.8 *In Vivo* Anticancer Efficacy of Prodrug Nanoassemblies in Solid Tumor

Mice bearing KB-3-1 tumors were used to evaluate the *in vivo* antitumor efficacy of the prodrug nanoassemblies. As shown in Figure 6A and 6B, compared with PBS group and PTX-OA/$TPGS_{2k}$ NPs group, Taxol showed a moderate antitumor effect with delayed tumor progression. In contrast, the mice treated with PTX-S-S-OA/$TPGS_{2k}$ NPs exhibited a significant decrease in tumor volume, with the tumor almost completely disappearing at the end of treatment (Figure 6B and 6C). Notably, PTX-OA/$TPGS_{2k}$ NPs exhibited poor

antitumor activity, showing no significant difference compared with the untreated control group (PBS). The inferior therapeutic effect of PTX-OA/$TPGS_{2k}$ NPs could be ascribed to its extremely slow release rate of free PTX, despite its long blood circulation (Figure 4) and high accumulation in tumor (Figure 5). On the other hand, the potent antitumor efficacy of PTX-S-S-OA/$TPGS_{2k}$ NPs could be attributed to several aspects: (i) good colloidal stability after PEGylation; (ii) long blood circulation time; (iii) high accumulation in tumor via EPR effect, owing to suitable size (~100 nm) and long-term blood circulation; (iv) efficient cellular uptake; and (v) rapid and differential release of active PTX molecules within tumor cells. These aspects cover almost all stages of drug delivery following intravenous administration, resulting in potent chemotherapeutic efficacy with decreased off-target toxicities.

TUNEL assay was used to evaluate whether Taxol, PTX-OA/$TPGS_{2k}$ NPs and PTX-S-S-OA/$TPGS_{2k}$ NPs induced apoptosis of tumor cells (Figure 6D and 6E). Significant PTX-induced apoptosis was observed in mice treated with Taxol (22.2%) and PTX-S-S-OA/$TPGS_{2k}$ NPs (64.1%), compared with that of PTX-OA/$TPGS_{2k}$ NPs (4.2%). Additionally, no significant change in body weight and the hematological parameters was observed in all the mice (Figure 7), Furthermore, no noticeable histological changes were observed in H&E-stained tissue sections of organs (Figure S8). This suggests that the redox-sensitive prodrug-nanosystem with potent antitumor activity elicited no significant off-target toxicities to major organs and tissues.

3. Conclusion

To develop advanced Nano-DDS for PTX delivery, we herein report a precisely self-assembled tumor-stimuli-responsive prodrug-nanosystem based on a disulfide bond inserted conjugate of PTX and oleic acid (OA) for improved chemotherapeutic efficacy. We designed a novel redox-responsive conjugates by bridging PTX and OA with disulfide bond (PTX-S-S-OA). An ester prodrug (PTX-OA) was used as the non-sensitive control. More interestingly, we found that both PTX-S-S-OA and PTX-OA could self-assembly into NPs. PEGylation with $TPGS_{2k}$ was utilized to achieve high stability and long blood-circulation of the prodrug nanoassemblies. As a result of the tumor-stimuli-triggered drug release, PTX-S-S-OA/$TPGS_{2k}$ NPs exhibited distinct superiority over both Taxol and PTX-OA/$TPGS_{2k}$ NPs, with the tumor almost completely disappearing in mice after the last treatment. Such a uniquely engineered small-molecule nanoprodrug-system with redox-responsive drug release provides great potential for further improving the chemotherapy of hydrophobic anticancer drugs.

4. Experimental Section

Materials

PTX was purchased from NanJing Jingzhu Bio-technology Co. Ltd, China. Paclitaxel injection (Taxol) was purchased from Hospira Australia Pty Ltd. Oleic acid (OA), dithiothreitol (DTT), ethylene glycol, phenylmethanesulfonyl fluoride (PMSF) and *N*-ethylmaleimide (NEM) were purchased from Aladdin, Shanghai, China. *N,N'*-dicyclohexylcarbodiimide (DCC) and 4-dimethylaminopyrideine (DMAP) were obtained

from Pukang Pharm Co. Ltd. (Zhejiang, China). Cell culture media RPMI 1640, DMEM, penicilline-streptomycin, and fetal bovine serum were purchased from GIBCO, Invitrogen Corp. (Carlsbad, California, USA). Hoechst 33342 was purchased from BD Biosciences, USA. 3-(4,5-dimthyl-2-thiazolyl)-2,5-dipphenyl-2H-terazolium bromide (MTT) and trypsin-EDTA were purchased from Sigma-Aldrich, USA. TUNEL assay kit was purchased from Promega, Madison, WI. VECTASHIELD with DAPI was purchased from Vector laboratories, Burlingame, CA. DiR was purchased from Life Technologies, USA. Tocopheryl Polyethylene Glycol 2000 Succinate ($TPGS_{2k}$) was synthesized according to our previous method.[30] All other chemicals and solvents utilized in this study were analytical or HPLC grade.

Synthesis of Conjugates

See the synthesis methods in Supporting Information.

Preparation and Characterization of Prodrug Nanoassemblies

8 mg of conjugates (PTX-S-S-OA or PTX-OA) and 1.2 mg of $TPGS_{2k}$ were dissolved in 1 mL of ethanol. The mixture solution was added dropwise into 4 mL deionized water under stirring (800 rpm). Self-assembly of NPs occurred readily. Ethanol in the nanosystems was then evaporated under vacuum at 30 °C. The nanoassemblies (PTX-S-S-OA NPs and PTX-OA NPs) without PEGylation were prepared similarly except for without adding $TPGS_{2k}$. Dye-labeled prodrug NPs were prepared similarly by co-assembling coumarin-6 or DiR with prodrugs in aqueous medium. The size, size distribution and zeta potential of the prodrug nanoassemblies were measured using Zetasizer (Nano ZS, Malvern Co., UK), and the measurements were repeated in triplicate. Additionally, the morphology of the nanoassemblies was observed by JEOL 100CX II transmission electron microscopy (TEM) (JEOL, Japan). Samples were stained with 2% uranyl acetate.

Colloidal Stability of Prodrug Nanoassemblies

The colloidal stability of non-PEGylated prodrug nanoassemblies and PEGylated prodrug nanoassemblies was evaluated by determining the mean diameter of the NPs. To investigate the stability under simulated physiological condition, prodrug nanoassemblies at a final concentration of 0.25 mg mL^{-1} were incubated in PBS (pH 7.4) supplemented with 10% of fetal bovine serum (FBS) for 12 h at 37 °C. To explore the long-term stability of the prodrug nanoassemblies, PTX-OA/$TPGS_{2k}$ NPs (2 mg/mL) and PTX-S-S-OA/$TPGS_{2k}$ NPs (2 mg mL^{-1}) were stored at 4 °C for three months. The particle size was determined at timed intervals by DLS.

In Vitro Hydrolysis of PTX from Prodrug Nanoassemblies

PTX hydrolyzed from prodrug NPs was determined by utilizing ethanol-containing PBS (pH 7.4) as the release medium. The particle dispersions (200 mg PTX equivalent) were incubated in 30 mL of release medium at 37 °C. At timed intervals, the derived PTX was determined by high performance liquid chromatography (HPLC), and the concentration of free PTX was obtained by using standard curves from the total peak area of the absorbance

at 227 nm. The *in vitro* hydrolysis of PTX from prodrug nanoassemblies in the presence of DTT was carried out similarly, except for the addition of DTT to the release medium.

Cell Culture

Human epidermoid carcinoma (KB-3-1), human lung carcinoma cell line (H460), and human ovarian carcinoma cell line (OVCAR-8) were obtained from University of North Carolina at Chapel Hill (UNC-CH) Tissue Culture Facility (TCF). The cells were cultured in RPMI 1640 medium supplemented with 10% (v/v) fetal bovine serum (FBS), penicillin (100 units/mL) and streptomycin (100 μg mL^{-1}) in a humidified atmosphere of 5% CO_2 at 37 °C.

Cytotoxicity Evaluation

The *in vitro* cytotoxicity of Taxol and prodrug nanoassemblies was investigated by MTT viability assay on KB-3-1, H460, and OVCAR-8 cell lines. Briefly, cells were incubated in 100 μL of complete culture medium in 96-well plates at a density of 5000 cells/well for 24 h. After pre-incubation, the cells were exposed to serial dilutions of Taxol, PTX-S-S-OA/$TPGS_{2k}$ NPs and PTX-OA/$TPGS_{2k}$ NPs, and further incubated for 48 h and 72 h. Untreated cells were utilized as control. At the end of the incubation, 20 μL of MTT (5 mg mL^{-1}) was added, and the plates were incubated for additional 3 h at 37 °C. The medium was then discarded, and the formed formazan crystals were dissolved in DMSO (200 μL). The absorbance in each individual well was determined at the wavelength of 570 nm with a multidetection microplate reader (Plate CHAMELEON V-Hidex). Each drug concentration was tested in triplicate.

Cellular Uptake

Cellular uptake was carried out on KB-3-1 cells. Cells were seeded in 12-well plates containing 1 mL of media at a density of 1×10^5 cells/well for 24 h. The medium was replaced with fresh medium containing free coumarin-6, coumarin-6-labled PTX-S-S-OA/$TPGS_{2k}$ NPs or PTX-OA/$TPGS_{2k}$ NPs with equivalent coumarin-6 concentration of 200 ng mL^{-1} for 0.5 h or 2 h at 37 °C. And the cells without any treatment were utilized as control. The cells were washed thrice with iced PBS, and the nuclei were counterstained by Hoechst 33342. Cells in culture medium were observed by using an Eclipse Ti-U inverted microscope (Nikon Corp., Tokyo, Japan).

For quantitative analysis, the cells were washed, harvested and suspended in PBS after incubation with free coumarin-6 or coumarin-6-labeled prodrug nanoassemblies. Untreated cells were utilized as control. Cellular uptake was analyzed by flow cytometry on a BD FACSCalibur instrument (Becton Dickinson).

Pharmcokinetics

According to the Guide for Care and Use of Laboratory Animals of Shenyang Pharmaceutical University, Sprague-Dawley rats (200–250 g) were utilized for the pharmacokinetics studies. All rats were randomly assigned to five treatment groups (n=6). Taxol, PTX-OA/$TPGS_{2k}$ NPs, PTX-OA NPs, PTX-S-S-OA/$TPGS_{2k}$ NPs, and PTX-S-S-OA NPs were administrated by intravenous (I.V.) injection with an equivalent PTX dose of 5 mg kg^{-1}. At timed intervals, about 0.3 mL blood was collected and centrifuged. The

concentration of prodrugs and free PTX in plasma was analyzed by a validated UPLC-MS-MS method on an ACQUITY UPLC™ system (Waters Co., Ltd., Milford, MA, USA).

Biodistribution

The biodistribution of prodrug nanoassemblies was investigated in KB-3-1 tumor-bearing nude mice (n=3). Until the tumor volume reached ~500 mm^3, mice were intravenously administrated with DiR solution, DiR labeled PTX-OA/$TPGS_{2k}$ nanoassemblies and DiR labeled PTX-S-S-OA/$TPGS_{2k}$ nanoassemblies at an equivalent DiR dose of 1 mg kg^{-1}. At 4 h or 24 h post injection, the mice were sacrificed for the observation of DiR accumulation in major organs and tumors by applying IVIS imaging system.

In Vivo Antitumor Activity

KB-3-1 cells (1×10^6 cells/100 μL) were inoculated subcutaneously to the female nude mice. When the tumor size was approximately 100 mm^3, KB-3-1 xenografts tumor-bearing nude mice were randomized to four groups (five mice per group): untreated control (PBS), free PTX (Taxol), PTX-OA/$TPGS_{2k}$ NPs and PTX-S-S-OA/$TPGS_{2k}$ NPs. These formulations were administrated through tail veins every other day for a total of five injections with an equivalent PTX dose of 8 mg kg^{-1}. Tumor volume and body weight were measured every day. Mice were sacrificed one day post-final injection, and serum was collected. The activities of aspartate transaminase (AST), alanine transaminase (ALT), blood urea nitrogen (BUN) and creatinine were assayed as indicators of hepatic and renal function. The tumor and major organs were collected and sectioned for further pathological study. Tumor cell apoptosis was then investigated by TdT-dependent dUTP-biotin nick end labeling (TUNEL) assay using an apoptosis detection kit (Promega, Madison, WI) according to the manufacturer's instructions, and tumor sections were stained by Hoechst 33342. All staining samples were observed with an Eclipse Ti-U inverted microscope (Nikon Corp., Tokyo, Japan). The formalin-embedded tissues were stained by hematoxylin and eosin (H&E) to identify the pathological change of major organs.

Statistical Analysis

All acquired data were presented with an average values and its standard deviation, shown as mean ± SD. Student's t-test and one-way analysis of variance (ANOVA) were utilized to analyze the differences of the groups, and $P < 0.05$ was considered statistically significant.

Supplementary Material

Refer to Web version on PubMed Central for supplementary material.

Acknowledgments

This work was financially supported by the National Basic Research Program of China (973 Program), No. 2015CB932100, the National Nature Science Foundation of China (No. 81273450, 81373336, 81473164), the Program for New Century Excellent Talents in University (No. NCET-12-1015), and NIH grant CA149387. The China Scholarship Council (CSC) is greatly appreciated for financially supporting Cong Luo's study in the United States (File No. 201408210110).

References

1. [accessed on 17 Jun 2016] http://www.who.int/cancer/prevention/en/index.html
2. Gammon JM, Dold NM, Jewell CM. Oncotarget. 2016; 7:15421. [PubMed: 26871948]
3. Bertrand N, Wu J, Xu X, Kamaly N, Farokhzad OC. Adv. Drug Deliv. Rev. 2014; 66:2. [PubMed: 24270007]
4. Luo C, Sun J, Sun B, He Z. Trends Pharmacol. Sci. 2014; 35:556. [PubMed: 25441774]
5. Jackman JA, Yoon BK, Li D, Cho NJ. Molecules. 2016; 21
6. Hackett MJ, Zaro JL, Shen WC, Guley PC, Cho MJ. Adv. Drug Deliv. Rev. 2013; 65:1331. [PubMed: 22921839]
7. Sivaprakasam S, Prasad PD, Singh N. Pharmacol. Ther. 2016
8. Bedikian AY, DeConti RC, Conry R, Agarwala S, Papadopoulos N, Kim KB, Ernstoff M. Ann. Oncol. 2011; 22:787. [PubMed: 20855467]
9. DiNardo CD, O'Brien S, Gandhi VV, Ravandi F. Future Oncol. 2013; 9:1073. [PubMed: 23902239]
10. Stuurman FE, Voest EE, Awada A, Witteveen PO, Bergeland T, Hals PA, Rasch W, Schellens JH, Hendlisz A. Invest. New Drugs. 2013; 31:959. [PubMed: 23345000]
11. Tao XM, Wang JC, Wang JB, Feng Q, Gao SY, Zhang LR, Zhang Q. Eur. J. Pharm. Biopharm. 2012; 82:401. [PubMed: 22728546]
12. Bradley MO, Webb NL, Anthony FH, Devanesan P, Witman PA, Hemamalini S, Chander MC, Baker SD, He L, Horwitz SB, Swindell CS. Clin. Cancer Res. 2001; 7:3229. [PubMed: 11595719]
13. Berquin IM, Edwards IJ, Chen YQ. Cancer let. 2008; 269:363. [PubMed: 18479809]
14. Kong X, Ge H, Chen L, Liu Z, Yin Z, Li P, Li M. Toxicol. in Vitro. 2009; 23:634. [PubMed: 19268700]
15. Menendez JA, del Mar Barbacid M, Montero S, Sevilla E, Escrich E, Solanas M, Cortes-Funes H, Colomer R. Eur. J. Cancer. 2001; 37:402. [PubMed: 11239764]
16. Kuan CY, Walker TH, Luo PG, Chen CF. J. Am. Coll. Nutr. 2011; 30:265. [PubMed: 21917707]
17. Fahrmann JF, Hardman WE. Lipids Health Dis. 2013; 12:1. [PubMed: 23295061]
18. Ke XY, Zhao BJ, Zhao X, Wang Y, Huang Y, Chen XM, Zhao BX, Zhao SS, Zhang X, Zhang Q. Biomaterials. 2010; 31:5855. [PubMed: 20430438]
19. Luo C, Wang Y, Chen Q, Han X, Liu X, Sun J, He Z. Mini Rev. Med. Chem. 2012; 12:434. [PubMed: 22303950]
20. Horwitz SB. Ann. Oncol. 1994; 5:S3.
21. Zhang Z, Mei L, Feng SS. Expert Opin. Drug. Deliv. 2013; 10:325. [PubMed: 23289542]
22. Bradley MO, Webb NL, Anthony FH, Devanesan P, Witman PA, Hemamalini S, Chander MC, Baker SD, He L, Horwitz SB, Swindell CS. Clin. Cancer Res. 2001; 7:3229. [PubMed: 11595719]
23. Lee FYF, Vessey A, Rofstad E, Siemann DW, Sutherland RM. Cancer Res. 1989; 49:5244. [PubMed: 2766292]
24. Yin Q, Shen J, Zhang Z, Yu H, Li Y. Adv. Drug Deliv. Rev. 2013; 65:1699. [PubMed: 23611952]
25. Wang Y, Liu D, Zheng Q, Zhao Q, Zhang H, Ma Y, Fallon JK, Fu Q, Haynes MT, Lin G, Zhang R, Wang D, Yang X, Zhao L, He Z, Liu F. Nano Lett. 2014; 14:5577. [PubMed: 25188744]
26. Wang J, Li S, Luo T, Wang C, Zhao J. Curr. Med. Chem. 2012; 19:2976. [PubMed: 22905345]
27. Chen W, Shi Y, Feng H, Du M, Zhang JZ, Hu J, Yang D. J. Phys. Chem. B. 2012; 116:9231. [PubMed: 22774761]
28. Wang J, Mao W, Lock LL, Tang J, Sui M, Sun W, Cui H, Xu D, Shen Y. ACS Nano. 2015; 9:7195. [PubMed: 26149286]
29. Reisch A, Klymchenko AS. Small. 2016; 12:1968. [PubMed: 26901678]
30. Wang J, Sun J, Chen Q, Gao Y, Li L, Li H, Leng D, Wang Y, Sun Y, Jing Y, Wang S, He Z. Biomaterials. 2012; 33:6877. [PubMed: 22770799]

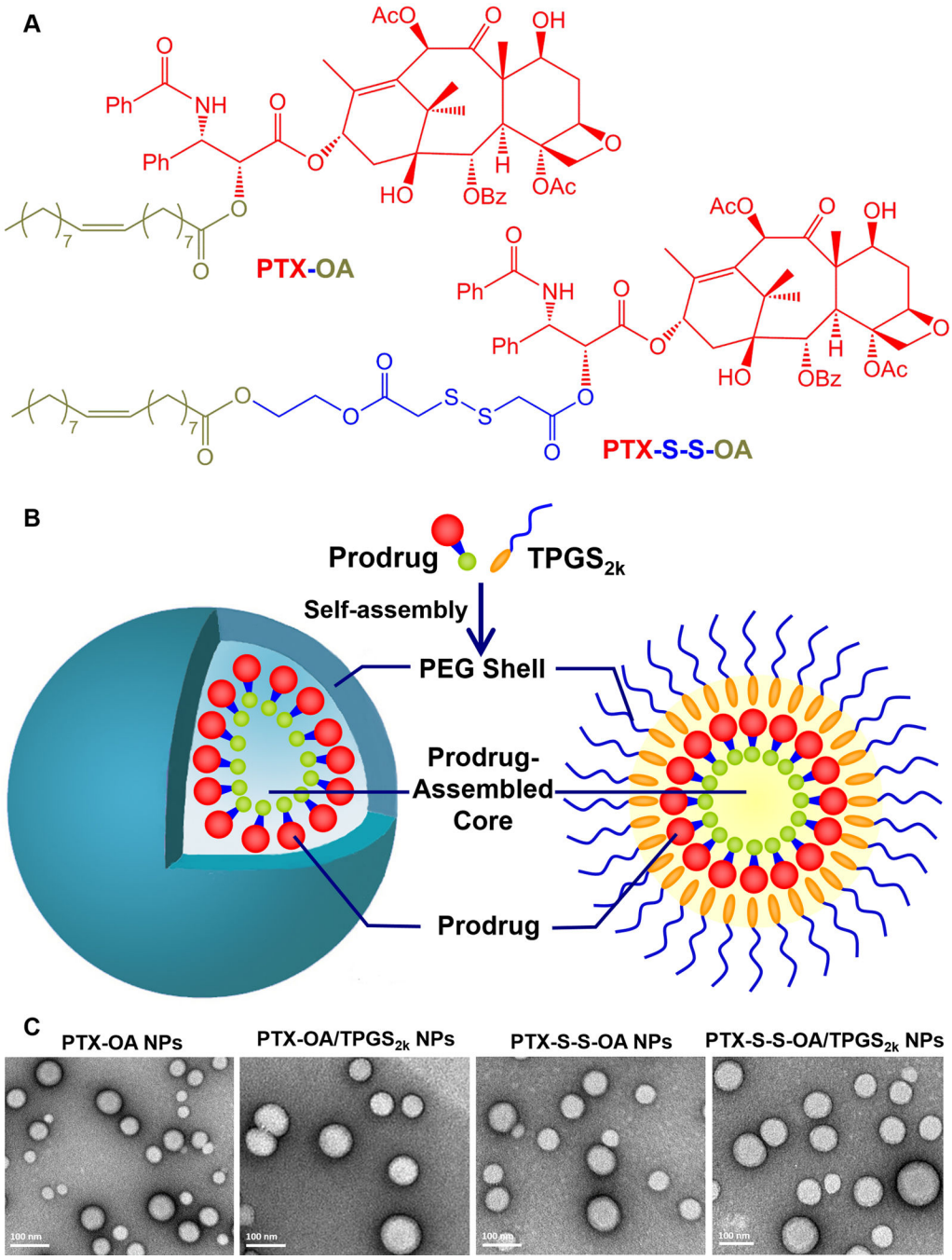

Figure 1.

(A) Chemical structures of PTX-OA and PTX-S-S-OA. (B) Schematic illustration of the assembly of PEGylated prodrug NPs. (C) TEM images of PTX-OA NPs, PTX-OA/$TPGS_{2k}$ NPs, PTX-S-S-OA NPs, and PTX-S-S-OA/$TPGS_{2k}$ NPs.

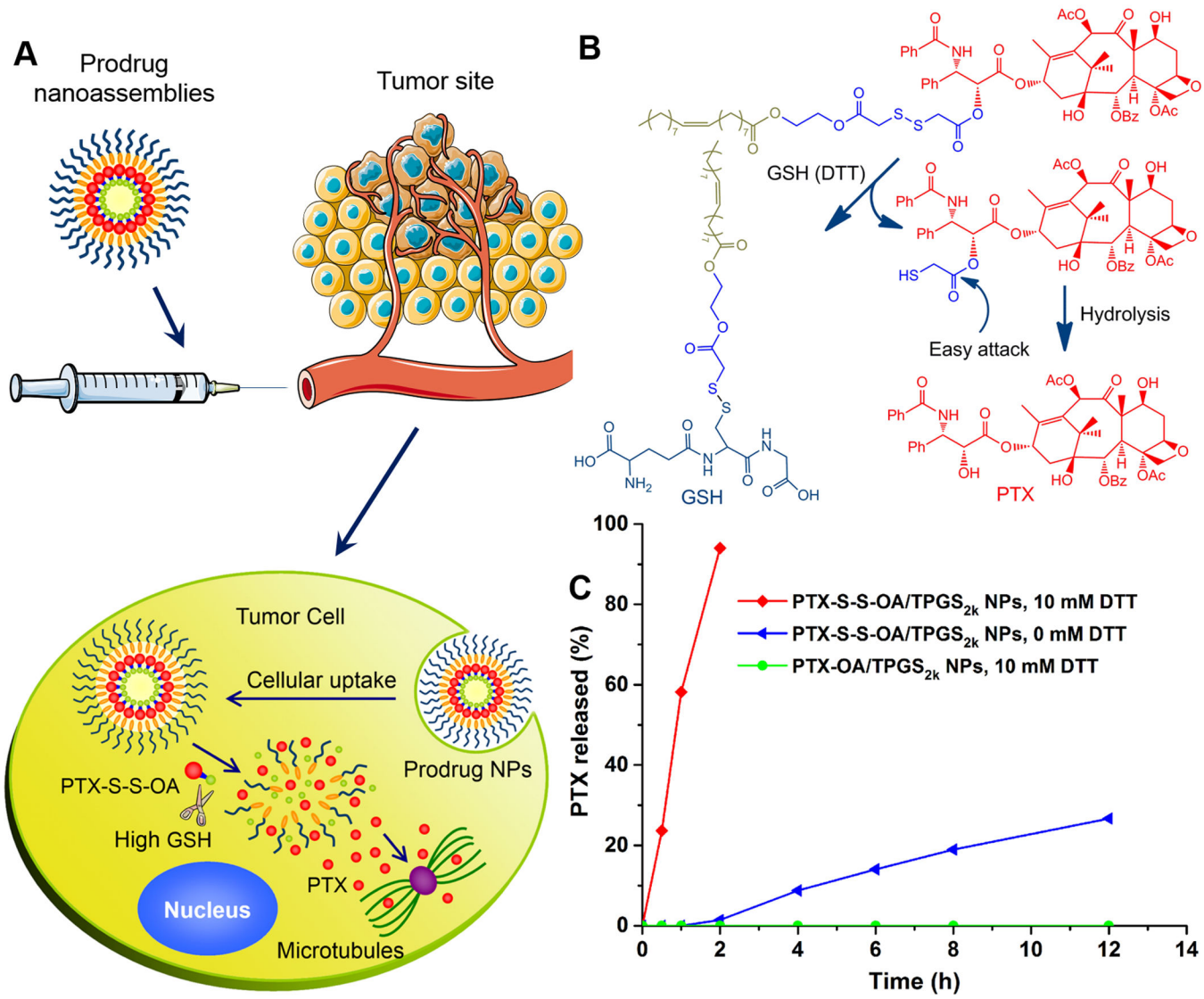

Figure 2.

(A) Schematic illustration of redox-responsive drug release of PTX-S-S-OA/TPGS$_{2k}$ NPs within tumor cells. (B) Redox-sensitive drug release mechanism of PTX-S-S-OA triggered by GSH (DTT). (C) PTX release from PTX-S-S-OA/TPGS$_{2k}$ NPs or PTX-OA/TPGS$_{2k}$ NPs.

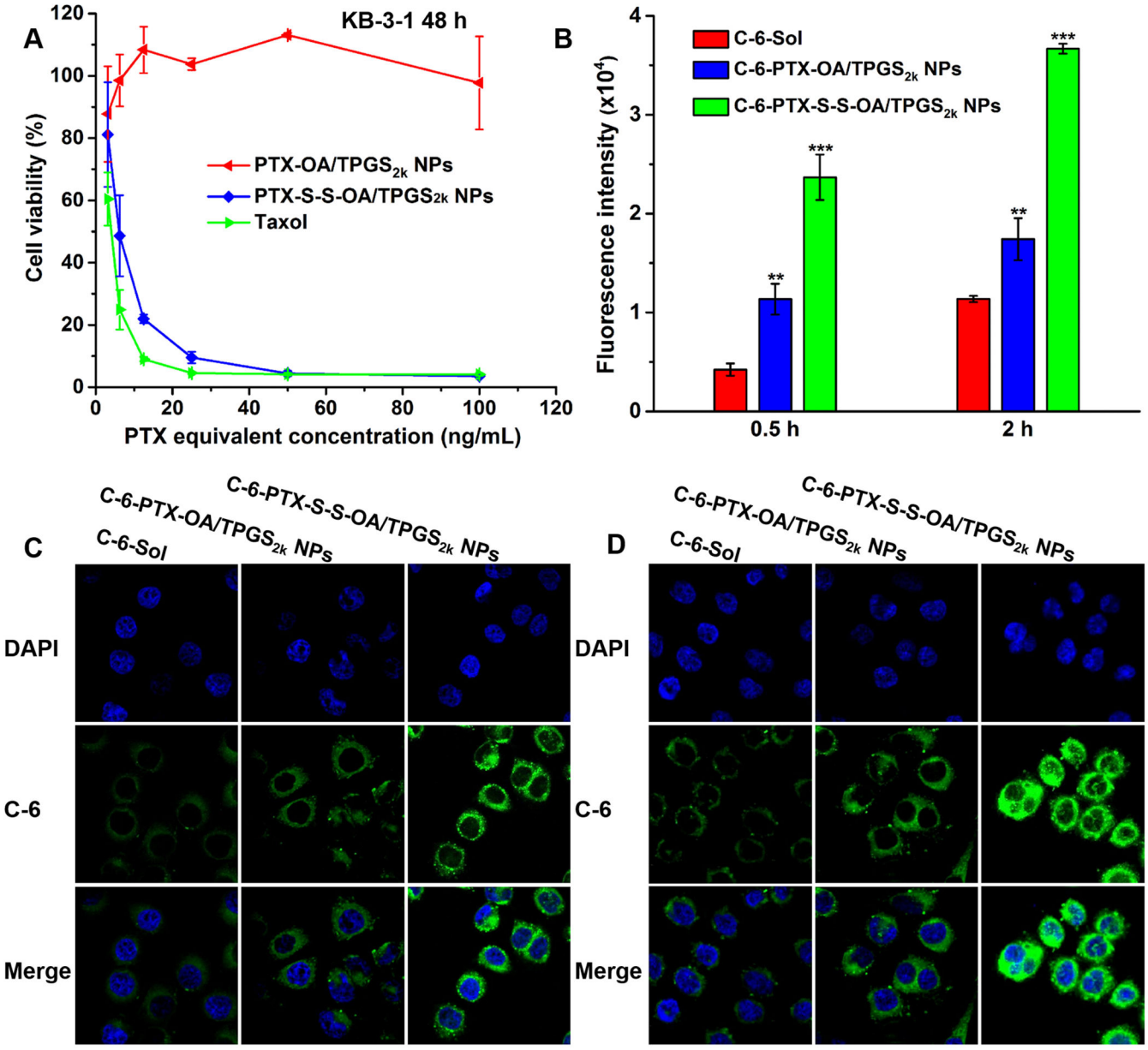

Figure 3.

(A) Representative dose-response curves of the MTT assays to KB-3-1 cell after 48 h treatment. (B) Flow cytometry results of cellular uptake in KB-3-1 cells after incubation with free C-6 or C-6-labeled prodrug nanoassemblies for 0.5 h and 2 h. Confocal laser scanning microscopy (CLSM) images of KB-3-1 cells incubated with C-6-Sol or C-6-labeled prodrug nanoassemblies (200 μg mL^{-1} equivalent C-6) for (C) 0.5h and (D)2 h. Difference from C-6-Sol group, ** $P < 0.01$, *** $P < 0.001$.

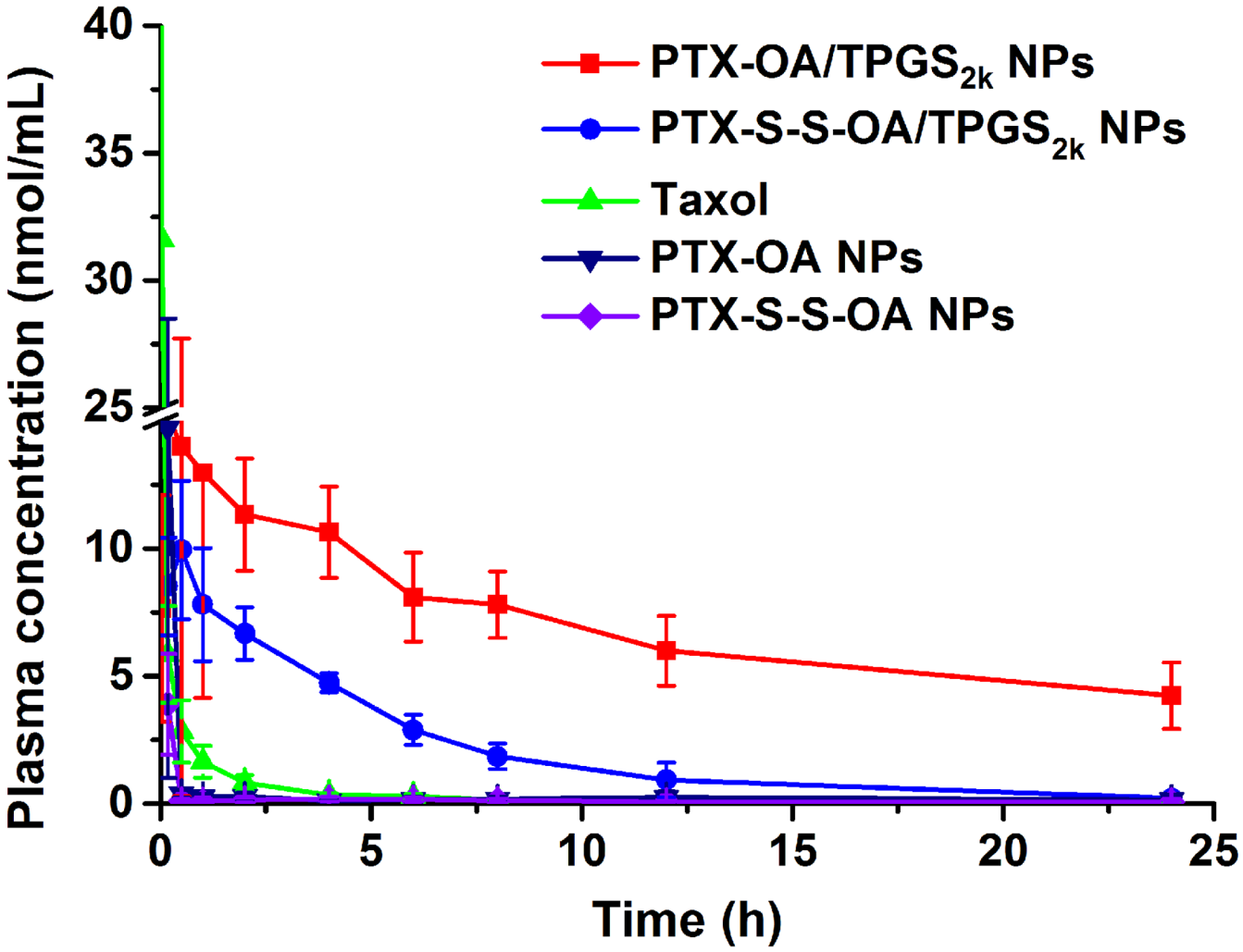

Figure 4.

In vivo plasma concentration-time profiles of Taxol, non-PEGylated prodrug nanoassemblies and PEGylated prodrug nanoassemblies following a single intravenous administration of 5mg kg^{-1} (PTX equivalent). (n=6)

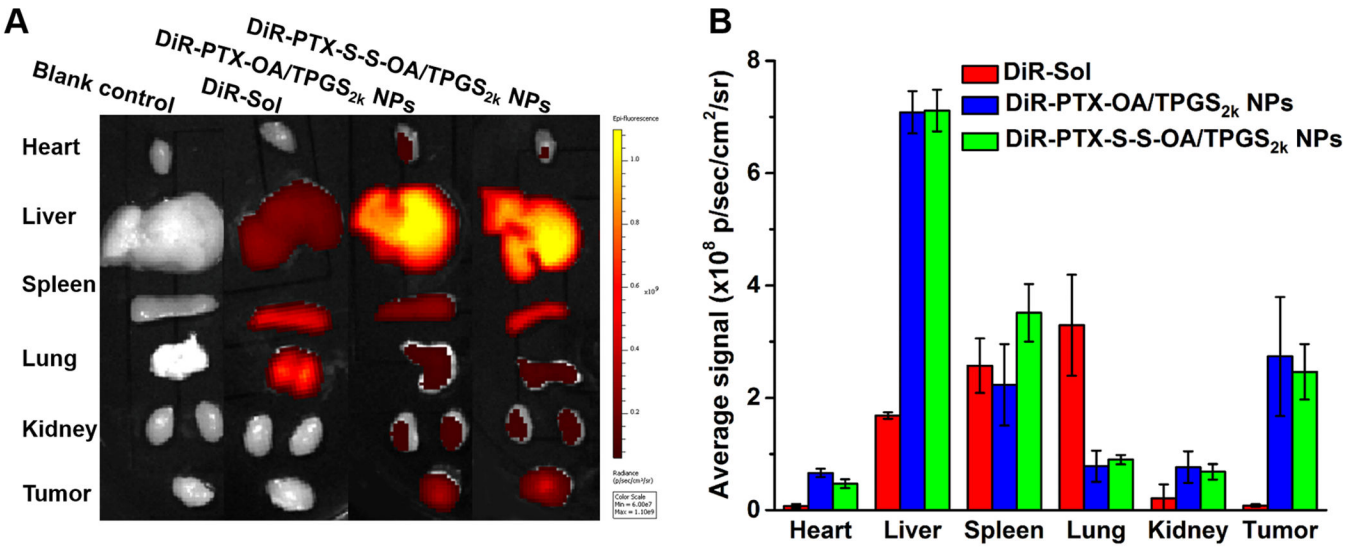

Figure 5.

In vivo distribution of DiR-labeled prodrug nanoassemblies (n=3). (A) Fluorescent imaging at 24 h. (B) Quantitative analysis of relative organ and tumor accumulation at 24 h. Data were analyzed by IVIS spectrum small-animal in vivo imaging system, error bars represent ± S.D.

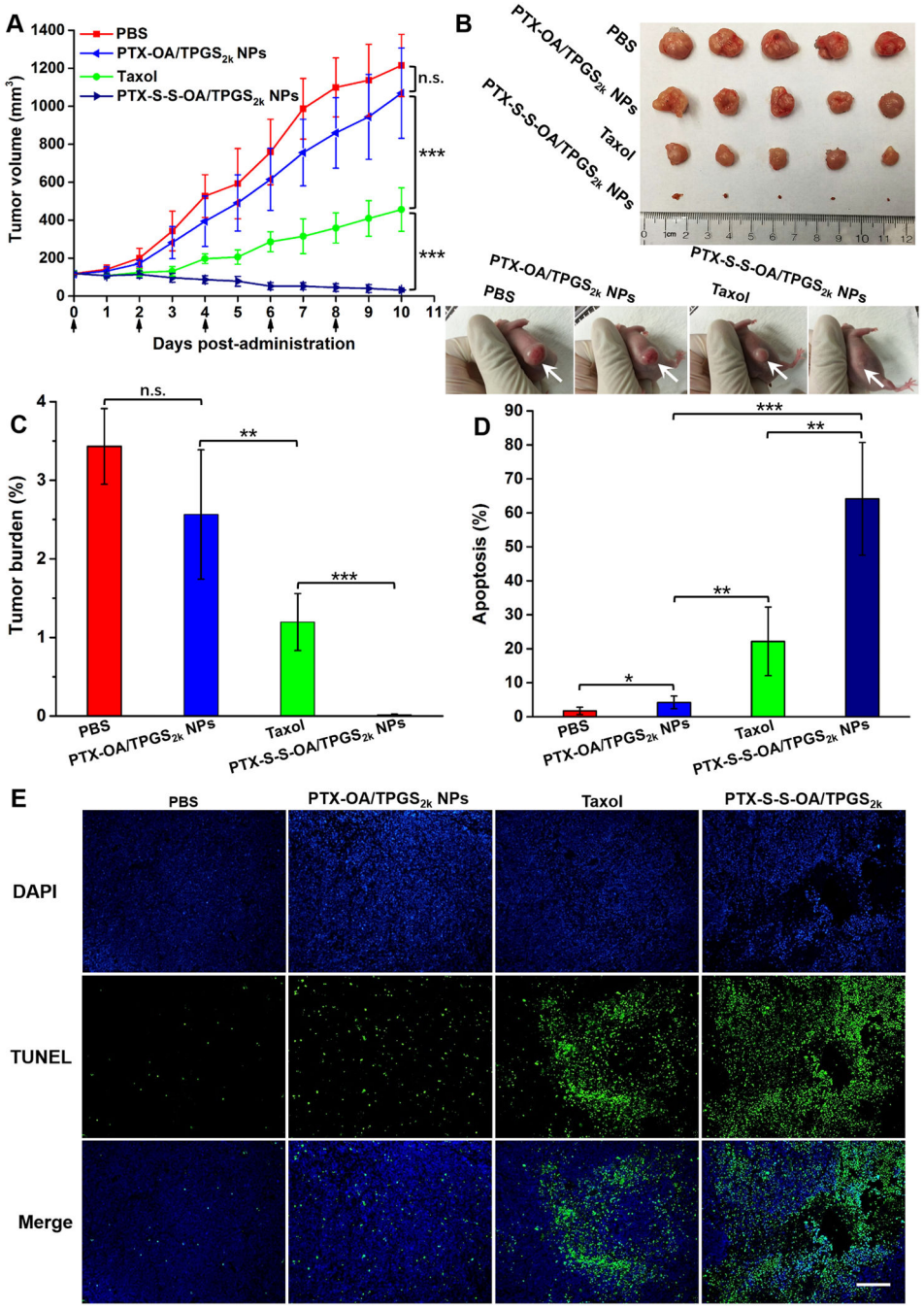

Figure 6.

In vivo antitumor activity of prodrug nanoassemblies against KB-3-1 xenograft tumors (n=5). (A) Tumor growth curves after injected with different formulations. (B) Pictures of tumors after last treatment. (C) Tumor burden, the weight of tumors was divided by the average body weight of mice. (D) TUNEL assay quantitative results of tumor sections treating with different formulations by Image J software (n=3). (E) TUNEL assay pictures of tumor sections treating with different formulations, scale bar represents 500 μm. The data are presented as means ± SD, * $P < 0.05$, ** $p < 0.01$ and *** $P < 0.001$.

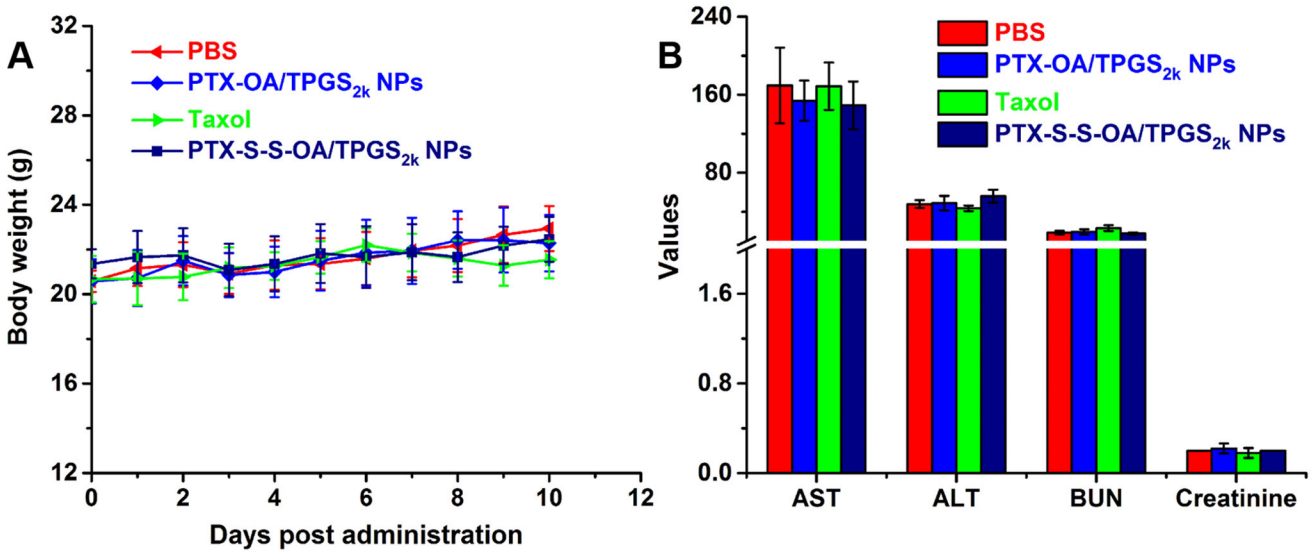

Figure 7.

(A) Body weight changes and (B) hepatic and renal function indicators of mice bearing KB-3-1 tumor xenografts after treatment. (n=5)